



HAL
open science

Virtual modeling of an ADAS radar

V J Palmier, S Prabakaran, F Faucher, A Serval, Alain Peden

► **To cite this version:**

V J Palmier, S Prabakaran, F Faucher, A Serval, Alain Peden. Virtual modeling of an ADAS radar. International Conference SIA Vision, Oct 2022, Paris, France. hal-03827097

HAL Id: hal-03827097

<https://hal.science/hal-03827097v1>

Submitted on 25 Oct 2022

HAL is a multi-disciplinary open access archive for the deposit and dissemination of scientific research documents, whether they are published or not. The documents may come from teaching and research institutions in France or abroad, or from public or private research centers.

L'archive ouverte pluridisciplinaire **HAL**, est destinée au dépôt et à la diffusion de documents scientifiques de niveau recherche, publiés ou non, émanant des établissements d'enseignement et de recherche français ou étrangers, des laboratoires publics ou privés.

Virtual modeling of an ADAS radar

V.J. PALMIER¹, S. PRABAKARAN¹², F. FAUCHER¹³, A. SERVEL¹, A. PEDEN¹⁴

1 : IRT SYSTEMX, 2 Bd Thomas Gobert, 91120 Palaiseau

2 : AVSIMULATION, 1 Cr de l'Île Seguin, 92100 Boulogne-Billancourt

3 : OKTAL-SE, 11 Av. du Lac, 31320 Vigoulet-Auzil

4 : IMT ATLANTIQUE, 655 Av. du Technopôle, 29280 Plouzané

Abstract: Safety has been an increasingly important issue for the development of autonomous cars. Within the 3SA project, the team is working on a simulation platform with the vocation to solve the problems related to the safety of the autonomous car. Regarding the perception, we propose methods for modeling ADAS sensors in constrained environments. Radars are part of these sensors. By their ability to detect targets with different parameters as range, speed or even angular position over a range up to 200 meters but also by their low sensitivity to meteorological conditions, radars provide several advantages for perception. However, some environmental parameters disturb the radar and affect its accuracy and reliability. Our team, a joint collaboration between academic (IMT Atlantique - IRT SYSTEMX) and industrial (Renault, AVSimulation, OKTAL-SE, STELLANTIS) partners, is working on the development of a physics based virtual radar model and on stress patterns in synthetic scenes. This paper addresses a particular validation step: the construction of a virtual radar model based on real characterization. To obtain an accurate radar model, our method combined theoretical radar concepts together with the use of a RF reference bench. We will see how real data of characterization of canonical forms obtained by the bench and the knowledge of the analytic RCS results of these forms allow to justify the results obtained with the real radar and to build the virtual model with a better level of accuracy.

Keywords: Radar, RCS, Simulation, Physics-based, ADAS, Autonomous Driving

1. Introduction

A sensor's physically based virtual modeling requires real characterization of this sensor in order to build a consolidated model. For an autonomous vehicle, the development of a virtual simulation synthetic environment and the validation of the system behaviour should take into external disturbances. Those external disturbances are due to phenomenon that can influence the decisions making process of the vehicle and the safety of its behaviour. In order to highlight some of these phenomena, while building the virtual radar model, the conception and the validation of these models require real data

acquisition according to a specific experimental protocol.

Within the 3SA project, a joint collaboration between academic (IMT Atlantique - IRT SYSTEMX) and industrial (Renault, AVSimulation, OKTAL-SE, STELLANTIS) partners, the team attached to the radar modeling, is working on the development of a physics based virtual radar model and on disturbance patterns in synthetic environment.

Firstly, this paper presents theoretical elements regarding radars. Secondly, it exposes the works for the characterization of the sensor and some real small targets characterized at IMT Atlantique Brest. Thirdly, it explains the transfer of this study to the virtual simulation through the modeling of the 3D replicas for the small targets and their physics-based modeling. Finally, after a benchmarking study between the experimental results and the simulation outputs, we draw conclusions about the state of the method and discuss its future perspectives.

2. Radar Cross Section

2.1 Definition and usages

Usually, the RCS is used to characterize objects to measure and to define their detectability. For the scope of this study, the methodology is inverted: some references objects with their known RCS for a real radar are used to model and validate a virtual radar. Data from real experimentation will enable to build the virtual radar step by step while ensuring the robustness. This consolidation via RCS measurement requires the use of known RCS analytical measurement targets. These objects characterized by simple geometries (cubic, sphere, rectangular plate, dihedral...) are said to be canonical.

For the exploitation of real data, the radar equation enables to obtain the radar cross section [2] with the exploitation of real measurements of the parameter $|S_{21}|^2$ explained as follows [1] :

$$|S_{21}|^2 = \frac{G_{TX}G_{RX}\lambda^2\sigma}{(4\pi)^3d^4} = \frac{P_{RX}}{T_{TX}} \quad [1]$$

d=distance between the target and the radar [m];
λ=wavelength [m]; P_{tx}=Transmitted Power [W];

P_{rx} =received power [W]; G_{tx} =transmission gain;
 G_{rx} =reception gain; σ = radar cross section [m²];
 $|S_{21}|^2$ =measured parameter

The equation [1] enables to obtain:

$$\sigma = \frac{P_{rx}}{P_{tx}} \frac{d^4 * (4\pi)^3}{G_{tx} * G_{rx} * \lambda^2} \quad [2]$$

In this expression, the distance d must be long enough to be in the far field of the object in order to have a correct value of RCS.

When the object is far enough to the radar, the measured RCS is considered to be in agreement with the theoretical value of RCS. This far field criterion is defined by the following formula where L [m] represents the biggest dimension of the target and λ represents the wavelength.

$$d \geq 2L^2/\lambda \quad [3]$$

2.2 Interest of the RCS Measurements

Usually, the RCS is used to characterize objects to measure and to define their detectability. For the scope of this study, the methodology is inverted: some references objects with their known RCS for a real radar are used to model and validate a virtual radar. Data from real experimentation will enable to build the virtual radar step by step while ensuring the robustness. This consolidation via RCS measurement requires the use of known RCS analytical measurement targets. These objects characterized by simple geometries (cubic, sphere, rectangular plate, dihedral....) are said to be canonical.

The theoretical determination of the RCS of canonical forms is based on the assumption of an "ideal" experimental configuration:

- The sensor is mono static: the same antenna acts as transmitter and receiver
- The target is positioned in the far field
- Radiation is considered to be isotropic
- There is no power loss

3. Measurements and data acquisition

3.1 Targets and analytic RCS results

For this part of the experimentations, six small targets are used. Five of them meet the following criteria:

- Their sizes: the object is small (a few centimetres for the largest dimension) enough to allow far field measurements inside an anechoic chamber described below.

- Their geometries: with a canonical form, the comparison with analytic results provides an additional reference point for the modeling.
- Their materials: the compositions are known and described in order to have a corresponding physical-based calculation.

The sixth target was a small metallic object with a simple geometry that can be compared with a car (see Figure 8). Its interest is to verify the robustness of the method with an unknown geometrical form.

In this paper, three of the six targets are presented for the scope of this paper: a sphere of four centimetres diameter, a dihedron with six centimetres side and the Small Metallic Car (SMC).

		Sphere (Diameter of 40 mm)	Dihedron (a=60mm h=59.5mm e=10.1mm)
F(GHz)	RCS expression	πr^2	$8h^2 a^2 \frac{\pi}{\lambda}$
79	Max RCS in m ²	0.001	14.913
	Max RCS in dB	-29.008	11.736
92.5	Max RCS in m ²	0.001	21.204
	Max RCS in dB	-29.008	13.264

Table 1 - Maximum RCS for the two objects with a canonical form

3.2 IMT RF Reference Bench



Figure 1 - Details of the quasi-monostatic configuration for the antenna with the connecting elbows

Transmission Frequency	79 GHz
Bandwidth	35GHz
Range resolution	4.2mm
Gtx	23,35 dB
Grx	23,35 dB

Table 2 - Description of the bench with the parameters of calibration

3.3 Real radar

In order to evaluate the radiation patterns of the power measurement of the radar and compare them to the datasheet, the radar is placed in a far field distance, facing a horn antenna connected to a vector analyzer in the far field. The radar is activated in transmission as follows:

- Each of the 3 T_x alone
- The 3 T_x together.

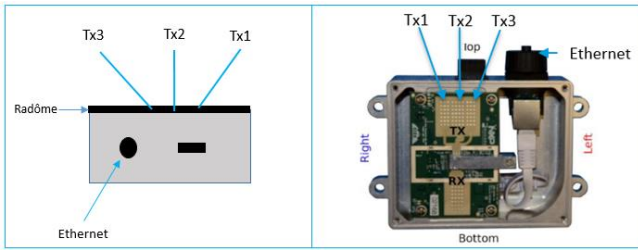


Figure 2 - RDK-S32R274 Reference Platform from NXP

The mixer located at the back of the horn induces a noise of around -20 dB. For the main lobes, the results showed a good match between the manufacturer's data and the measurements but the noise induced by the mixer and the vectorial analyzer was too important to obtain the global diagrams.

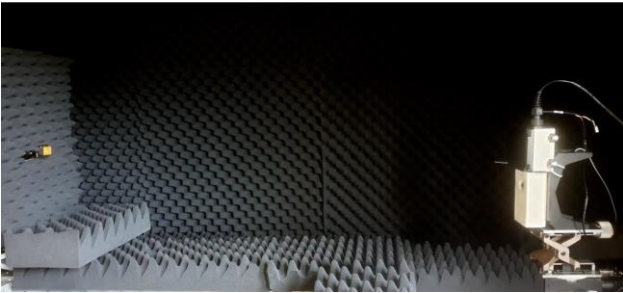


Figure 3 – Measurement protocol of antenna patterns in the azimuthal plan

Acquisitions of the RCS were made with two different configurations of activation of the transmit antenna: T_{x2} only and 3 T_x together. For both, parameters of acquisition are the same and presented in the following table.

Transmission Frequency	79 GHz
Tx activated	T_{x2} or 3 T_x together
Bandwidth	2GHz
Range resolution	75mm
Maximal range of detection	19,13m

Table 3 - Parameters

In this paper, only the results with the central antenna T_{x2} will be presented. This choice is justified by the following facts:

- It is the central antenna
- It is the only one for which the datasheet diagrams in elevation and azimuth were available
- It is the one offered greater measurement dynamics compared to the noise specific to the measurement device

3.4 Description of the experimental design scene

In order to ensure the most optimal experimental conditions possible, the measurements were carried out in an anechoic chamber, thus ensuring the elimination of parasitic reflections and the maximum reduction of environmental noise.

For the respect of the theory of the Radar Cross Section, each target is placed at a far field distance defined regarding its size.

f (GHz)	Far field distance (m)		
	Sphere	Dihedron	SMC
79	0.85	1.90	1.32
92.5	0.99	2.23	1.55

Table 4 - Minimum distance of the far field criteria for each target

The anechoic chamber is 2 meters long and after subtracting the occupied length reference bench system, there remains a distance amplitude of 1.6 meter. That means the dihedron couldn't be in far field distance inside the anechoic chamber. Thus, for the respect of the far field theory for each target, the experiment was split into 2 configurations:

- Configuration 1: Target and measurement system are both in the anechoic chamber at a distance of 1.6 meter each other. During the acquisitions, the chamber was closed.

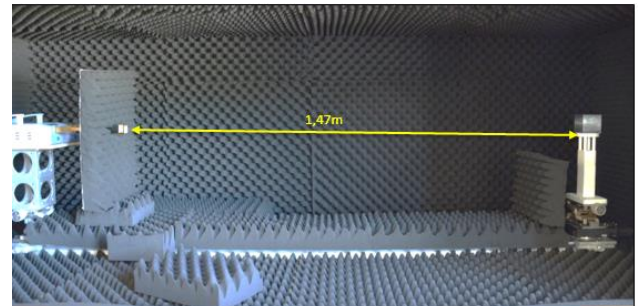


Figure 4 - Picture of the opened anechoic chamber with the installation of the reference bench. Distance between the front of the horns and a target Add approximately 13cm to the distance to take into account the connecting elbows of the horns (reference bench)

- Configuration 2: The target is in the anechoic chamber and the measurement system is outside the chamber at a distance of 3m (Figure 8). During the acquisition, the chamber was opened.

The acquisition system and the target were at the same height in both configurations validated with a LASER. The declination of the system is zero. The acquisition system is fixed and the target is in rotation. The target is placed on a foam support of permittivity substantially equal to 1 positioned on a rotary motor with a precisely calibrated rotation pitch.

The rotation pitch is defined and chosen according to the target studied.

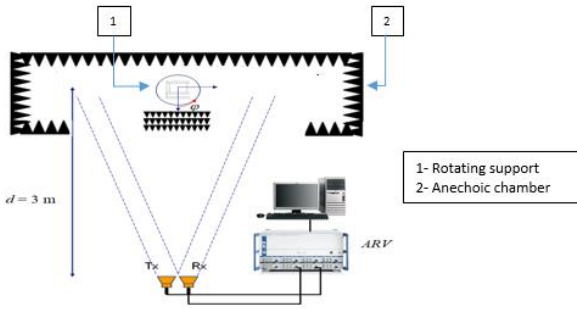


Figure 5 Measurement configuration with the bench outside the chamber

The protocol is the same for both devices. To ensure the experimental protocol, when it takes the place of the reference system, the radar is placed at 1.6m of the target to take into account the distance included by the connecting elbows of the reference one. The targets are changed between two acquisitions without moving the system {rotary motor + support}. Before changing the measurement system, all the targets are tested first.

3.4 Results and comparison of the real experimental results

At the time of writing this article, the values obtained via the radar are still being studied: so, they are not presented here.

Although the looks RCS of the 3 targets are the same for the theory, the reference bench and the real radar, some discrepancies between the theoretical values and the measurements were to be expected.

These errors come from both the point of view of the reference bench and the point of view of the radar. Indeed, at the section 2.2, we introduced the fact that the theory was built in an ideal case but in real experimentation both for the environment and for in relation to the sensor itself, the framework cannot be ideal.

The reference bench is not really mono static contrary to the theory and its radiation is not isotropic; the alignment between the center of the transmission antenna and the center of the target is not perfect. This error leads to a mean error between the specified maximum gain and the one deduced from the RCS measurements of the sphere of 1.45 dB

The real radar is not mono static and its radiation is not isotropic.

The anechoic chamber:

- In the configuration 1, the anechoic chamber has some leaks that could lead to minimal additional signal losses as well.

- In the configuration 2, the anechoic chamber is opened which create a large leak. Moreover the edge of the chamber, at the joint, has a metal coating and there are losses caused by the reflections outside the chamber.

The support, although its low permittivity, have its signature observable in the measurement.

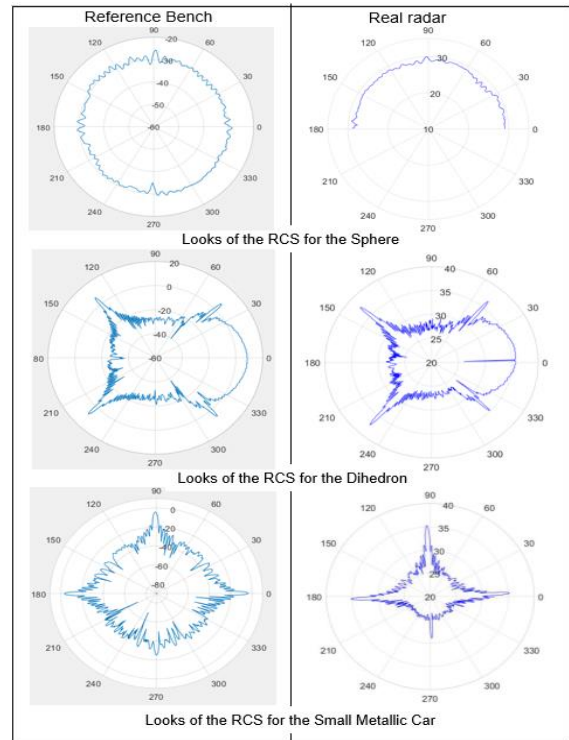


Figure 6 Looks of the RCS at 79GHz – reference bench (cf. 3.2) – real radar (cf. 3.3). The measurement for the sphere with real radar were made on 180 degrees because of the duration of the acquisitions and the sphere form looks perfectly

4. Simulation of radar data

The simulation goal is to provide data which areas realistic as the phenomenon we want to model. Generally, in the automotive field, it relies on having a description of 4 elements:

- A detailed environment which comprises the terrain
- Actors including the behaviour of the ego and all the targets surrounding it in the detection range
- A perception model characterized by the sensors and all its specifications

In this case, for RCS simulation, there is no environment or ego to describe because we focus only on radar interaction with its targets. Thus, the next parts of this paper will only deal with objects modeling, sensor description and acquisition.

4.1 Object modeling

The first step is the definition of a workflow of object modeling for physical sensor simulation. Objects are defined by their geometries (3D models) and their material descriptions (reflection, specular, rugosity, etc.). This definition can be written in a .BDD file which is the file extension of SE-WORKBENCH.

In order to obtain this file for a specified object, the applied workflow is described in the Figure 7. The objective of this workflow is to have different formats corresponding to the different software that are used in the simulation. These files are generated from the same source 3D model which is then declined in different formats. These toolchains are described in the next paragraph.

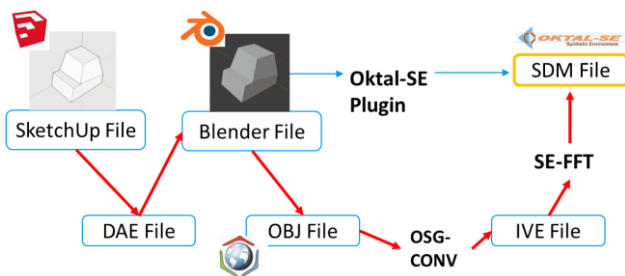


Figure 7 - Applied workflow of 3D modeling

The modeled objects are listed in the table below.

Sphere (40 mm diameter)	Dihedron (width of 60 mm)	Small Metallic Car (width of 50 mm)

Figure 8 - Calibration objects and their corresponding 3D Geometry (Blender)

4.2 Physical simulation with SE-WORKBENCH

The physical RCS simulations were performed thanks to the SE-RAY-EM software which is the EM kernel of SE-Workbench-RF product line. SE-RAY-EM solver uses asymptotic methods coupled to ray tracing in order to compute scattered electromagnetic fields at the bench and radar bandwidth. This method is relevant for the automotive domain since the size of the objects is large compared to the wavelength (a few millimetres for 79GHz). In the case of complex targets and large 3D scenes, the full wave methods are not applicable for several reasons. Where a few

GHz is a high limit for “exact” solutions used on this type of objects, it is almost a low limit in terms of physical validity for asymptotic methods. The standard computation range addressed by this method is roughly between 1 to 100 GHz on complex 3D scenes that suit to automotive scenarios. Moreover, asymptotic method coupled to ray tracing produces results that are very similar to the “exact” methods for a very much lower computation time [1]. Ray-tracing is done through the Shooting and Bouncing Rays (SBR) technique that has been further optimized to calculate efficiently the intersections between rays from the transmitter towards the 3D target and back to receiver. Figure 9 shows that rays are traced from the transmitter through a grid (pixels). The intersections of these beams are computed.

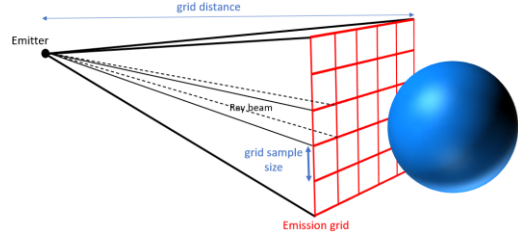


Figure 9 - Ray-tracing grid

There are two types of interactions that are based on three formulations [2]:

- Geometrical Optics (GO) when the beam is reflected by a metallic or dielectric surface.
- Physical Optics (PO) towards the reception points at each interaction.
- Equivalent Current Methods (ECM) for computing edge diffraction toward the reception points.

Since the canonical targets are metallic pieces, the Perfect Electric Conductor (PEC) material was the only model involved under the following simulations. In order to be able to properly compare the results with the measurements, the following parameters set of the simulations matches the measurements conditions:

- The longitudinal distance between the antenna and the target
- The vertical alignment of the target according to the antenna
- The distance between the phase center of the emitter and the receiver antenna
- The path of the antenna around the target
- The number of angles computed (same azimuth sampling)
- The same bandwidth

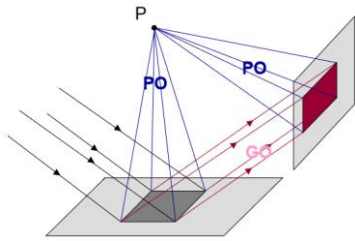


Figure 10 - Principle of beam interactions [1]

The results of the three simulations presented in this section were performed with the same set of ray-tracing parameters given on the Table 5 in the next section. Each scenario of the three simulations only comprises a single target, the source antenna and a reception point that take place within a free space environment. Hence, as soon as SE-RAY-EM has computed the complex EM field, it is simple to get the RCS value from the radar equation. This equation leads to the expression given below.

$$\sigma(\theta) = \frac{(4\pi)^2 R^4}{2 Z_0 P_t} |Er(\theta)|^2 \quad [4]$$

Where $\sigma(\theta)$ is the radar cross section (m^2) for a given azimuth angle θ ($^\circ$), $|Er(\theta)|$ is the module of the complex polarised electric field (V/m) computed by SE-RAY-EM at the reception point for a given θ , Z_0 is the free space impedance (around $120\pi \Omega$), P_t is the transmitted power of the source ($1W$) and R the source-target distance (m).

Figure 11, Figure 12 and Figure 13 respectively show the plots of the car shape target, the dihedron and the sphere. First, we can say that the curves of these plots fit the expected analytical ones. Since the simulations were performed very close to the near field limit, the value of σ_{max} diverges a little from the expected analytical values. However, as long as the radius distance increases, the σ_{max} converges very close to the theoretical value (up to 10^{-3} -for this set of parameters). These simulations have several goals, one of them is to check the maximum value computed by the kernel in order to compare it with the expected analytical value. Besides, the plots enable us to compare the profile of the computed curves with the measurements in order to check the validity of the solver for different wavelength from 79GHz to 92.5GHz.

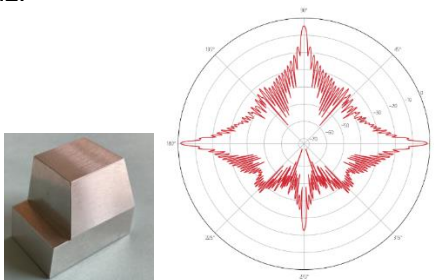


Figure 11 – RCS (θ) plot results of the car shape object

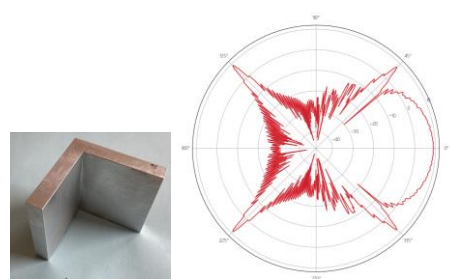


Figure 12 – RCS (θ) plot results of the dihedron

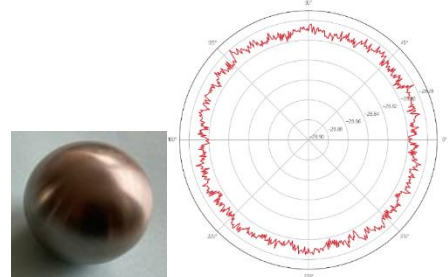


Figure 13 - RCS (θ) plot results of the sphere

Furthermore, many different measurements were performed across many different simple geometries will help us to identify the magnitude of the gap between the measurements and the simulation. This information will be ultimately used to check the validity of more complex geometries such as vehicles, traffic signs, bicycles as well as pedestrians. The ray tracing parameter set given in the figure 12 is purposely demanding for this latter reason as well. Finally, the next section will show that these simulations can be performed again in an automotive simulation context through SCANeR Studio and as a validation of the software integration of SE-RAY-EM.

4.3 Applying in SCANeR Studio

The previously presented tool SE-RAY-EM has been integrated in the software solution SCANeR Studio from AVSimulation. The goal of such an integration is to apply the physics-based sensor modeling in the field of automotive simulation. During this study, the goal has been to use the integrated tool in SCANeR Studio to reproduce the simulations that have been done with the SE-RAY-EM tool, in order to validate the fact that the theoretical value simulated by the physical-based software can be approached with another platform.

The context of the simulation is different because it is based on the scenario description of SCANeR Studio. A scenario needs an ego vehicle, a terrain and the actors surrounding the ego. Here, the goal is to measure an RCS surrounding the whole object. Hence having an ego vehicle equipped with a correctly parametrized sensor. The ego has a circular trajectory around the object in order to surround every

angle of the object at the precise distance (as described in Figure 14)

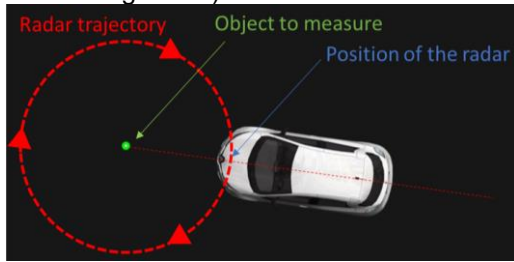


Figure 14 - SCANer Studio view of the measurement for RCS scenario

4.4 Results and comparison of the simulations

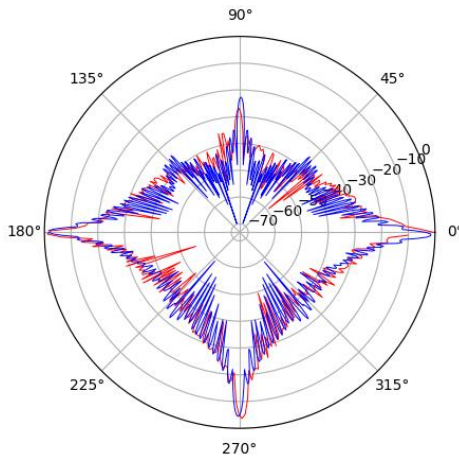


Figure 15 – Comparison of both the simulations for the small metallic car (red: SCANer and blue: SE-WORKBENCH)

When applying the simulation process to the three objects of the study, the results (an example is shown in Figure 15) obtained are similar to the simulated RCS with SE-WORKBENCH. The computation core model is the same for both tools but we can highlight some disparities due to the different context and some differences in the simulation parameters used with SCANer.

First approximation come from the scenario itself. In SCANer simulation, the ego vehicle is moving around the object applying a small velocity due to the rotation of it. This velocity can imply small dopplers. These can be avoided by stopping the car before each measurement for each angle but the impact of such dopplers is negligible.

The other approximation comes from the simulation parameters: for the integration of the SE-RAY-EM tool into SCANer Studio, some simplifications have been made to be more adequate and easier to use for an automotive use case. The table below shows the differences between SE-WORKBENCH and SCANer Studio parameters.

	SCANer	SE-WB
Grid sample size	10^{-2} m	10^{-3} m
Grid subdivision level	2^1	2^4
Curve sampling precision	1°	0.5°

Table 5 - Ray-tracing parameters set

Some parameters are less accurate in SCANer Studio because such precision is not necessary in the automotive field. In spite of this simplification, the scenario is able to get an accurate representation of the RCS even for very small objects of 4 to 5 centimetres.

5. Comparison of simulated data with real data

At this stage of development, the virtual RADAR is not finalized. However, as it appears in chapter 4 for this paper, the virtual model of the reference bench is in a good state of achievement. The discussion about the comparison of simulation data with real data will be about the real data of the benchmark.

5.1 Results

Figure 16 describes a superposition of the results of RCS obtained with OKTAL-SE, with SCANer and we compared them with the measurements that have been done at IMT Atlantique with the reference bench. The 3 results have the correct shape and the measurement shows that the model used (in SE-WORKBENCH and then in SCANer Studio) are relevant regarding the measured value in the anechoic chamber.

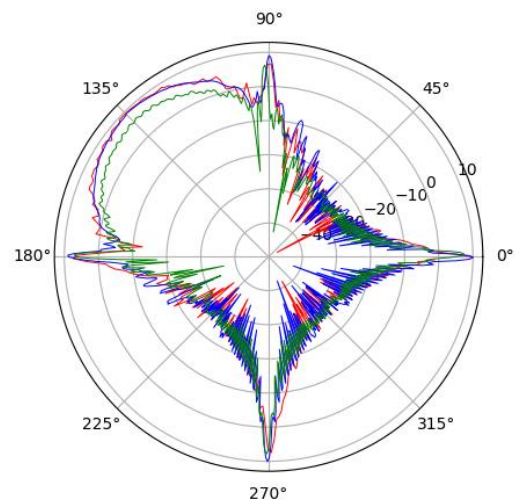


Figure 16 - Layering of the RCS of the dihedron for the 3 measurement sources (blue: OKTAL-SE, red: SCANer Studio and green: IMT)

Angle	0°	90°	135°	180°	270°
Ref Bench	7.4	6.2	6.4	7.2	7.8
SCANeR	7.7	7.7	7.5	7.7	7.7
SE-WB	7.8	7.9	8.4	7.9	10.1

Table 6 - Local max values of RCS (in dBm²) simulated and measured for remarkable angles of the dihedron

RCS max in dBm ²			
	Sphere	Dihedron	SMC
Theory	-29	11,89	
Ref Bench	-30.1	8,24	-4,33
SCANeR	-27.7	11,22	-0,51
SE-WB	-28.8	10,99	-1,57

Table 7 - Results of the maximum and of the mean RCS for each object

	RCS mean error	
	Dihedron	SMC
Ref Bench/Theory	3.65 dB	
SE-WB/Theory	0.9 dB	
SCANeR/Theory	0.67 dB	
SCANeR/SE-WB	0.36 dB	0.27 dB
IMT/SCANeR	2.23 dB	2.037 dB
IMT/SE-WB	1.87 dB	2.34 dB

Table 8 - mean error (in dB) of the RCS between different data sources (only with the max RCS for the theory)

5.2 Discussion

The results are satisfying. Although, the gaps of the maximum RCS between the results of simulation and the theory are small, they are more important between the reference bench and the simulation.

These differences can be more precisely observed in Table 6 which shows local maximum values of RCS around different angles (each face of the dihedron and the center corner of it at 135°).

The identified causes can be due to:

- The causes identified in section 3.5
- In simulation (SCANeR and SE-WORBENCH), the antennas are defined as isotropic antennas unlike the real ones. This choice explains the good scores between the theory and the simulation radiation in theory is defined as isotropic (cf. section 2.2)

The first results exposed in this paper are satisfying because SE-WORKBENCH and SCANeR correctly depicts the shape of the RCS expected with the real RCS measured. The construction of virtual non isotropic antenna could enable to increase the similarity between the real and the simulations. In the same way, the simulations could deviate from the theory. This demonstrates the relevance of using two sources of reference to build the virtual model.

6. Conclusion

To conclude, this first step of the method development shows a possible and robust workflow to validate radar modeling using simulation and two sources of references (theory and experimentations). The use of RCS reference value helps verifying the correct behaviour and quantification in our sensor model in controlled use case (anechoic chamber). Furthermore, the methodology used is validated from the step of object modeling to the step of parametrization of the sensor with two different toolchains: on one side, the physics-based tool (SE-WORKBENCH) and on the other side, its integration in a software platform (SCANeR Studio) allowing us to address multiple automotive use cases.

This workflow can now be applied for more complex scenarios implying more complex objects such as real cars, pedestrians and adding an environment to the measurement (movements of the objects and actors, and surrounding infrastructures).

7. Acknowledgement

Thanks to Charaf-Eddine SOURIA for having contributed to the definition of this method.

This work has been supported by the French government under the "France 2030" program, as part of the SystemX Technological Research Institute.

References

- [1] J. Latger, T. Cathala: "Millimeter waves sensor modeling and simulation", 2015.
- [2] N. Douchin, J. Latger, T. Cathala, R. Marechal: "Simulating complex environments for the assessment of millimeter waves sensors", 2016.
- [3] N. Douchin, C. Ruiz, J. Israel, HJ. Mametsa SE-Workbench-RF: "Performant and High-Fidelity Raw Data Generation for Various Radar Applications", 2019.
- [4] IRT SystemX - Simulation for the Safety of Systems in Autonomous Vehicles (3SA Project): <https://www.irt-systemx.fr/en/projets/3sa/>.
- [5] OKTAL-SE: <https://www.oktal-se.fr/>
- [6] AV Simulation: <https://www.avsimulation.com/>

8. Glossary

RCS: Radar Cross Section

SMC: Small Metallic Car